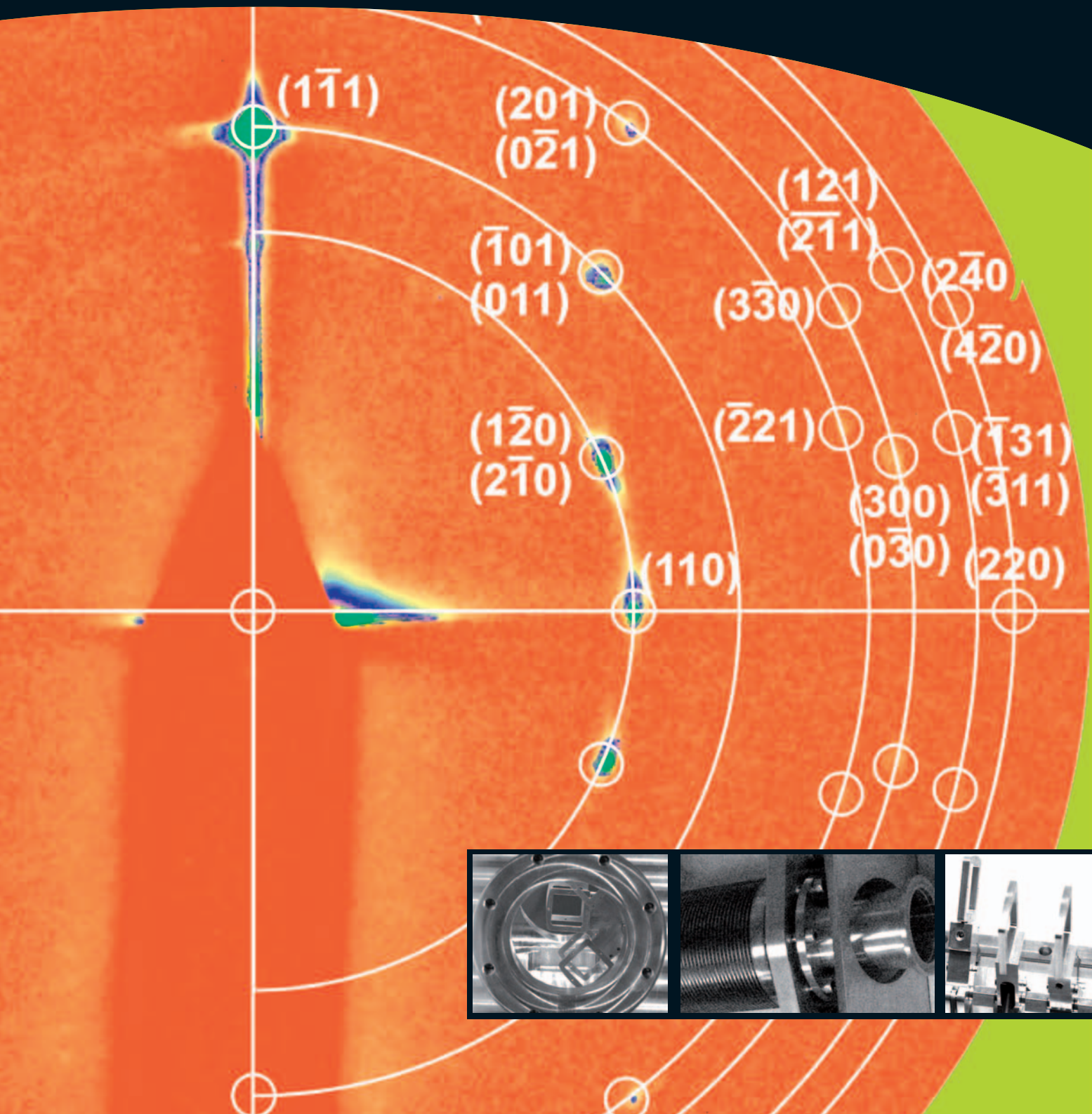


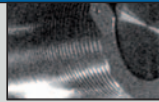
XMaS

NEWSLETTER



2009





3

Workshop on Multiferroics Research

4

Instrumentation developments

8

Scientific Highlights

18

News round-up

19

Guidelines for beam-time applications



Another year of XMaS operation has passed (can anyone really believe that we opened the beamline in autumn 1997?) and has been marked by a number of changes in personnel, some scary events and lots of good science. In May 2009 we said goodbye to David Paul who retired after being associated with the project from its inception – we first employed David in 1993 and based him at the Daresbury laboratory to work with David Laundry on the design of our diffraction beamline for magnetic materials – it was later when it was named XMaS and much later when we realised that there was a world of materials science beyond magnetic materials. David was wholly responsible for the design of the optics and it is probably no exaggeration to say that he still knows where every bolt and flange is located. However, he no longer needs to remember it all since, after 12 years as our Beamline Coordinator, he is enjoying retirement in rural Lincolnshire. His successor is no stranger; it is Laurence Bouchenoire who first came to XMaS as a PhD student and won a beamline scientist position in 2002. She took over from David this summer and became our XMaS Beamline Coordinator but retains some of her former research activity. Simon Brown assumes David's role of Beamline Responsible.

Six months earlier we had welcomed Oier Bikondoa, who had previously worked on ID01, to a post jointly funded by the project and the DIAMOND Light Source. The role was designed to increase our expertise in the surface diffraction side of XMaS and then transfer that expertise to the DLS. In fact, in the "musical chairs" that followed David's retirement, Oier has taken the Beamline Scientist post that Laurence vacated and we are currently seeking a new appointee to that joint post. The rest of the familiar faces remain: they just get a bit older (and wiser?).

What about scary moments? Well, 2008/9 saw a recession and a rapid drop in sterling. This prompted a lot of discussion with EPSRC about our future: would the beamline have to close one year early? We buy most of our equipment and pay for all the services we take from ESRF in euros, our funding is in sterling and the exchange rate dropped from 1.47 € = £ 1 in autumn 2007 to near parity in early 2009 (and not much more now). Well, all's well that ends well; EPSRC is underwriting sufficient of the predicted shortfall for us to be able to keep XMaS operating at full tilt until autumn 2012. More generally EPSRC is changing the way it considers funding for facilities such as ours categorised as "mid range". The first call for new and repeat funding was summer 2009

and, given the fact that XMaS is funded up to September 2012, it is perhaps not surprising that our case was put to one side this time. We have to hope that EPSRC does not completely run out of funds after the next government's Comprehensive Spending Review, anticipated to follow rather rapidly after the 2010 UK election, because we will need to address the funding issue in 2011.

A more dramatic scare occurred in March 2009 when the great XMaS fire threatened to end any worries about funding not lasting to 2012. A failed water supply (it's not that simple really) led to the melting of parts of the 1 Tesla electromagnet and the subsequent flooding of the hutch and the evacuation of the whole ESRF ring. We have always praised Huber diffractometers as robust instruments but now we can indeed testify that they are fire and flood proof. The only permanent damage was the complete destruction of the electromagnet, now replaced by one with twice as many safety cut-outs and sensors! The diffractometer only needed a clean before Huber's engineers pronounced it in good health and we were able to heave a great sigh of relief. There are probably strange and wonderful fungi growing beneath the steel clad floor but the radiation will get them!

Most of the beamline's instrumental developments are discussed later in this Newsletter, but we note here that two more XMaS inventions, the magnetically operated attenuators and the piezo flipper have been licensed for commercial sale.

During 2009 and, after much agonising, we agreed to go ahead with an upgrade to cryogenic cooling of the monochromator in order to reap the benefits of the ESRF's upgrade programme. Thus over the Christmas 2008 shutdown the goniometer spindle was re-engineered for cryocooling whilst retaining the flexibility for water cooling. We always knew that this would be a major project, both in terms of cost and complexity, but we only realised late in the day that supply pipes carrying liquid nitrogen are not as compact or as "bendy" as water pipes and so now you see that the optics hutch has a new set of doors alongside the goniometer to facilitate loading and alignment of the crystal cage and goniometer spindle. All the cryo-plant is in place and the final step will be the crystal cage and cooled crystal set, of which more later in this Newsletter, together with all the exciting stuff about your science.

Malcolm Cooper and Chris Lucas

Workshop on Multiferroics Research



The Functional Materials Group at the National Physical Laboratory (NPL) and XMaS co-hosted the first UK workshop on x-rays and neutrons in multiferroic research on 17th June 2009. The NPL group specialises in developing characterisation methods for dielectric, piezoelectric, ferroelectric and multiferroic materials. Multiferroics are multifunctional materials, combining two or more of the ferroic ordering parameters (ferroelectricity, (anti)ferromagnetism and ferroelasticity). An important subclass of these materials, magnetoelectrics, are remarkable because of their potential application for new multifunctional devices, including novel sensors, spin-valves, biosensors and memory storage – our understanding of the full industrial impact of these novel materials is only just emerging.

A series of talks showing recent progress in this field was kicked off by Neil Mathur (Cambridge) who gave an introduction to multiferroic, magnetoelectric and ferroelectric phenomena, detailing examples of materials properties such as bismuth ferrite, which is a good room temperature ferroelectric. Crystallography studies of this material were presented by Phil Lightfoot (St. Andrews) and Tim Comyn (Leeds), the former using neutron diffraction measurements to determine the atomic structure of the high temperature phases, and the latter investigating the effect of different sample processing techniques on the crystal symmetry. Doping bismuth ferrite with lead titanate results in a mixed phase compound that has strongly ferroelectric and piezoelectric. It is also possible to “switch on” the magnetic ordering by means of an in-situ hydrostatic pressure.

The use of magnetism to control the polarisation was discussed by Des McMorrow (UCL) who used non-resonant x-ray scattering and x-ray polarimetry to deduce the magnetic structure and domain population of the multiferroic TbMnO₃. The same techniques were employed by Peter Hatton (Durham) to look at the magnetism of a different terbium manganese oxide, TbMn₂O₅. The magnetic structure refinements using these techniques however, often rely on complementary neutron studies, and some examples of these in the wider class of manganese oxide materials RMn₂O₅ were presented by Carlo Vecchini

(ISIS). Geetha Balakrishnan (Warwick) discussed how the non-ferroic SmMnO₃ compound could be “tuned” into multiferroicity by doping with yttrium to force the crystallographic structure into the part of the RMnO₃ phase diagram occupied by TbMnO₃ and DyMnO₃ – well known multiferroic compounds. She concluded by presenting neutron scattering data on the frustrated Kagome staircase compounds nickel vanadate and cobalt vanadate – previously studied for their interesting magnetic order, and only recently discovered to be ferroelectric.

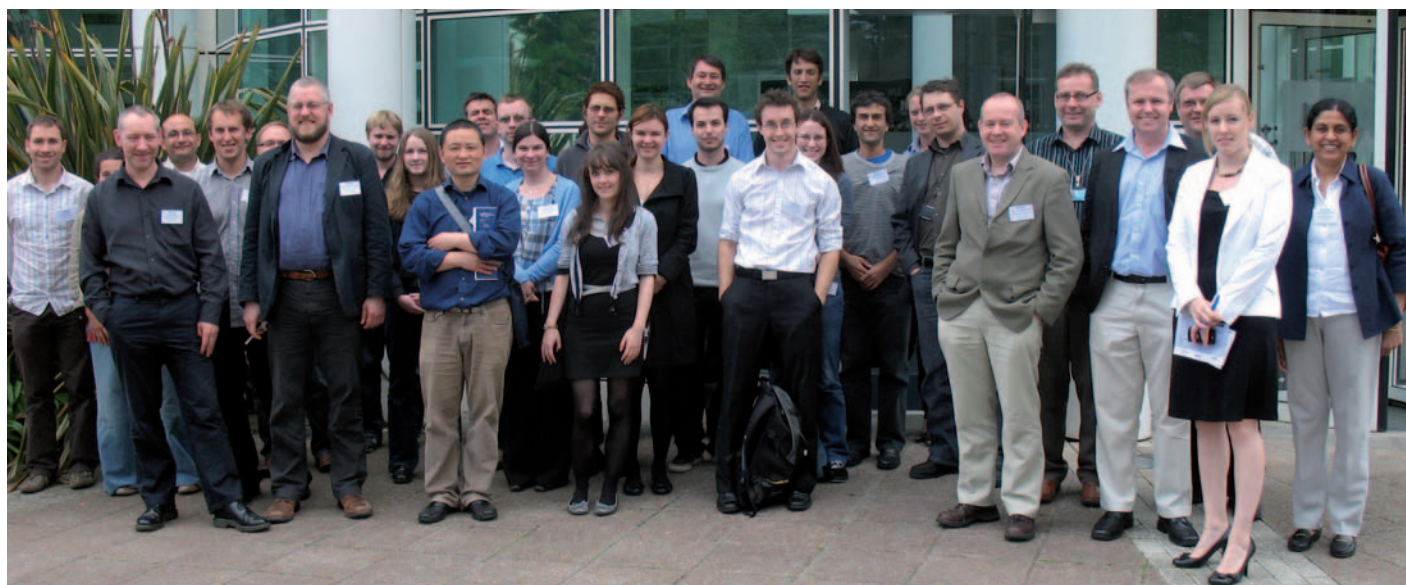
The workshop concluded with presentations by Mark Stewart (NPL) on the experimental procedures required to characterise ferroelectric materials and how these should be employed in a neutron or x-ray experiment, and Paul Thompson, who gave an overview of the measurement capabilities at the XMaS beamline, which is ideally suited to the study of multiferroics. Finally the afternoon session finished with an open discussion chaired by Bob Cernik (Manchester). The group ascertained the main experimental interests in this field focus on the ability to perform in-situ magnetoelectric and piezoelectric measurements.

A subsequent wiki site* has been created that aims to centralise all the information required to perform a multiferroic neutron/x-ray experiment – from best practice guides on sample preparation and electrode deposition techniques, to experimental beamline descriptions designed to help users choose the right measurement technique for the right experiment. Additionally, users are encouraged to contribute information on their experimental successes and failures, so that their experience will help the rest of the community avoid making costly mistakes.

This very successful workshop was a first milestone for the development of fundamental research in the field of multiferroics. The system to carry out in-situ PE loops at XMaS has been recently commissioned by the NPL Functional Materials Group. More details can be found in the article “Electric Field capability” later in this Newsletter.

*http://interactive.npl.co.uk/multiferroics/index.php/Main_Page

Participants at the X-ray & Neutron Scattering in Multiferroics Research Workshop at NPL.



Monochromator upgrade

With the forthcoming ESRF upgrade, the storage ring current is expected to be increased from 200 mA to 300 mA, with a corresponding increase of 50% in the incident power on the first crystal. The current water cooled system can dissipate approximately 200 W and further cooling power requires cryogenic liquids. Cooling monochromator crystals with liquid nitrogen (LN₂) increases the thermal conductivity of silicon and decreases its thermal expansion coefficient. A standard ESRF cryo-cooler system has therefore been installed recently on the beamline. The present Vacuum Generators goniometer has been retained, but the main shaft has been broadened to accommodate the wider LN₂ tubes. The wall of the optics hutch has also been modified by the addition of a door to enable the monochromator vessel, which now has a longer goniometer shaft and less flexible LN₂ cooling lines, to be opened. A mezzanine has also been constructed for the cryogenic cooling plant.

A new crystal cage is being designed to access energies from 2.2 to 15 keV. It will be based on the same simple concept as the current water cooled version and the two will be completely interchangeable. It is proposed to use a side cooled Si(111) first crystal, approximately 50 mm thick, which will allow good thermal conduction from the silicon to the LN₂-cooled copper plates of

the cryo-cooler. The second crystal will also be cryogenically cooled. This second crystal assembly will be kinematically mounted with three linear actuators having a step resolution of 50 nm. This will preserve the 20 mm constant exit height.

Low energy optimisation

When the beamline was conceived in the mid-1990's, there was a strong interest in the scattering community for actinide magnetism, particularly for performing resonant x-ray scattering at energies as low as the U M₅ absorption edge (~3.5 keV). The original beamline design therefore minimized the number of absorbing elements such as beryllium windows and air paths to limit the attenuation of the low energy photons. More recently, however, there has been considerable interest in using lower energy x-rays to study 4d systems including for example ruthenate materials, where magnetic and orbital ordering occurs, heavy fermion superconductors and nanostructures involving Pd (see the highlight in this Newsletter). Thus there is a strong demand to access the L_{2,3} edges of the 4d elements (2.97 to 3.33 keV) for resonant scattering experiments. Presently there is still 850 μm of beryllium in the beamline, 500 μm of which is the window in the front end, 100 μm separating the mirror and the monochromator and a further 250 μm window used to isolate the high vacuum (~5×10⁻⁹ mbar) section of the beamline

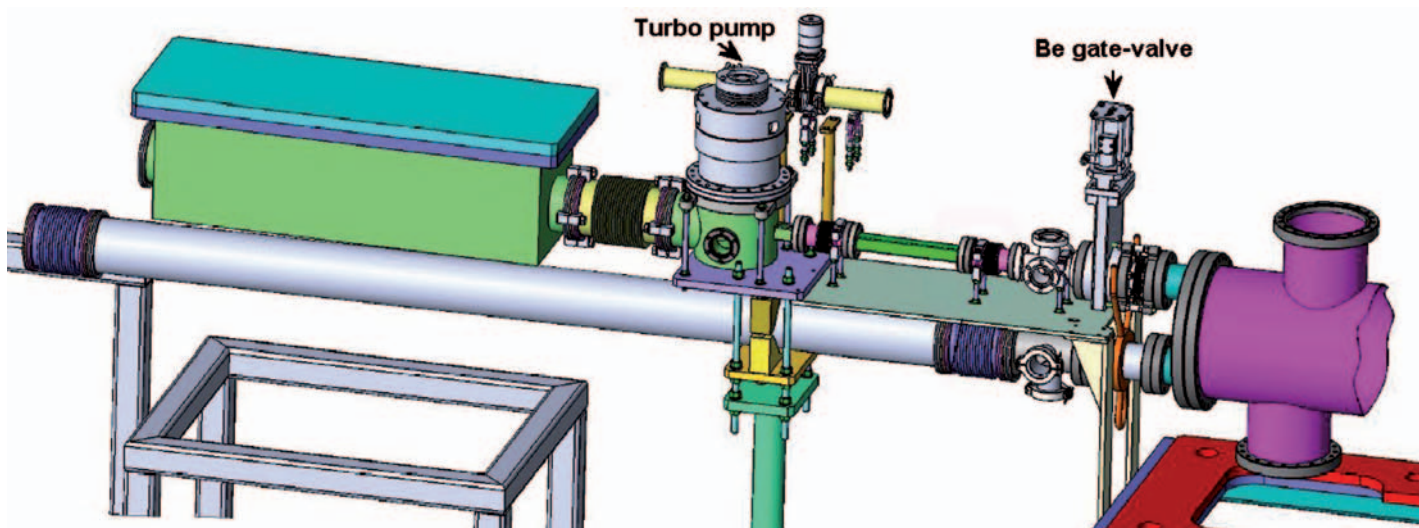


Figure 1: Drawing of the differential pumping section for windowless operation between the front end and the detector.



containing the optical components from the coarse vacuum (1×10^{-3} mbar) of the user area. These beryllium windows severely limit the available flux for energies lower than 4 keV and their presence is the limiting factor for experiments at these low energies.

After discussions with the ESRF Front End group, we have determined that the 500 μm beryllium window can be reduced to one of only 250 μm and still provide the necessary protection for the storage ring vacuum. This reduction of 250 μm will immediately yield an increase in flux of 250% at 3 keV. The removal of the 100 μm thick beryllium between the mirror and the monochromator is also envisaged. Secondly, upgrades to the vacuum system in the experimental hutch are planned to enable windowless operation from the front end, i.e. from the optics, via the sample environment, up to the detector. A differential pumping system is to be installed between the vacuum systems in the optics and the user sections of the beamline. A small cross sectional area tube with a low conductance will be placed between the final slit vessel and the harmonic rejection mirrors in the experimental hutch (**Figure 1**). This assembly is pumped by a large turbo pump, easily achieving pressures below 1×10^{-6} mbar in the experimental hutch section and ensuring that the vacuum in the optics section is not degraded. The removal of the current 250 μm isolation window will increase the flux available at 3 keV by a further 170%. For conventional hard energy scattering windowless operation is not required and it remains prudent to protect the vacuum in the optics section. Thus the current isolation window will be re-mounted onto a gate-valve enabling a quick transition between windowed, and windowless operation.

Thirdly, the phase plate flipper assembly will be incorporated into a vacuum chamber to remove a section of air-path plus kapton windows. Finally, the beamline team have been in communication with the staff at beamline X13A, NSLS (Brookhaven National Laboratory) who commissioned an in-vacuum avalanche photodiode. It is proposed to build a similar prototype mounted onto a KF style vacuum flange, enabling windowless detector operations on XMaS.

At low photon energies, considerable attention also needs to be paid to the sample environment. A typical dispex used for x-ray diffraction, which reaches temperatures below 15 K, will usually have both vacuum and radiation beryllium shrouds. If both the incoming and outgoing beam paths are considered, the thickness of these shrouds can easily add up to some 1500 μm and cause prohibitive beam attenuation at low photon energies (**see Figure 2**). A range of windowless sample environments that can

be mounted onto a standard dispex and Huber diffractometer have been designed to allow a wide range of scattering studies. An in-vacuum system incorporating an electromagnet and an array of photodiodes has been designed for combined reflectivity and spectroscopic studies. Gate valves are used to isolate the cryostats from the windowless beamline vacuum system during such routine operations such as sample changes etc.

Improved Grazing Incidence

The XMaS user community is developing a growing interest in grazing incidence small and wide angle scattering – GI-SAXS/WAXS –, primarily for the study of polymers. A new arrangement for combined (GI)SAXS and WAXS experiments has been designed. A rail, directly attached to the base of the diffractometer, will allow the manual positioning of a 2D detector from ~ 0.1 up to ~ 1.80 m from the sample. The detector could also be displaced both vertically and horizontally. The air path between sample and detector will be minimised by using a set of adapted SAXS tubes from Daresbury and the motorised beam stop will be in vacuum to reduce stray scattering. An additional point or 2D detector could be placed on the diffractometer's detector arm to simultaneously measure the WAXS signal. This setup can be combined with diverse XMaS sample environments.

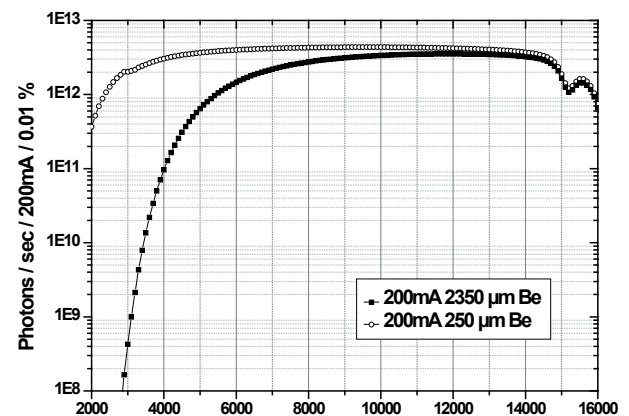


Figure 2: Comparison of the current flux available with 2350 μm of beryllium to that of only 250 μm .

Electric field capability

Multiferroics materials are currently seeing a resurgence of interest, with proposed applications from computer memory to extremely sensitive magnetic detectors but there is a need to characterise samples fully in order to understand them and develop improved device materials. X-rays are a powerful tool to elucidate the origin of structural changes but they cannot necessarily determine the direction of polarisation in ferroelectrics. The classic demonstration that a sample is ferroelectric is to measure a spontaneous polarisation that is switchable by the application of an electric field – namely a P-E hysteresis loop. The XMaS team has been collaborating with the NPL Functional Materials Group in order to set up an in-situ system where P-E loops and x-ray diffraction data are collected simultaneously by means of a fast acquisition card (Figure 3). The MUSST card developed by the ESRF can collect the data in each separate channel at rates up to 20 MHz. This development will help users to carry out studies of ferroelectrics and multiferroics in complex conditions such as 4 T magnetic field and electrical potentials up to 2 kV in the 2 K environment already available at XMaS. The commissioning of this system, plus some initial usability and verification tests have recently been carried out without the X-ray beam by Markys Cain and Mark Stewart from NPL. Tests now need to be carried out with live beam.

P-E loops have been measured on soft lead zirconium titanate (PZT). Figure 4 shows very clear ferroelectric switching with a large remnant

polarisation that makes this type of material useful as a non volatile memory element. In fact this material had been previously poled at elevated temperature explaining the slightly non-symmetric polarisation behaviour; one direction is still more stable than the other. If the material were to be de-poled by heating above the Curie temperature, then the P-E loop would display a 2-fold rotational symmetry.

Figure 5 shows measurements on a ceramic multilayer capacitor which has piezoelectric (Barium Titanate based) ceramic layers sandwiched between magnetostrictive nickel electrodes. These commercially produced devices happen to show magnetoelectric coupling, but are normally used as capacitors at a maximum rating of 16 V. However, if we apply a much higher voltage (250 V), equivalent to a field of 250 kV/cm, we observe ferroelectric behaviour. This material, which had not been previously poled has much lower remnant polarisation. The curve is thereby no longer offset about the zero polarisation axis and is more symmetrical.

The results of these tests represent the verification of the electrical component of the system presented in Figure 3. Work is continuing to improve the ease of use of the setup and remove minor electrical noise issues, but it is now ready for users.

For more details on the P-E measurement system contact Mark Stewart at NPL, e-mail: mark.stewart@npl.co.uk.

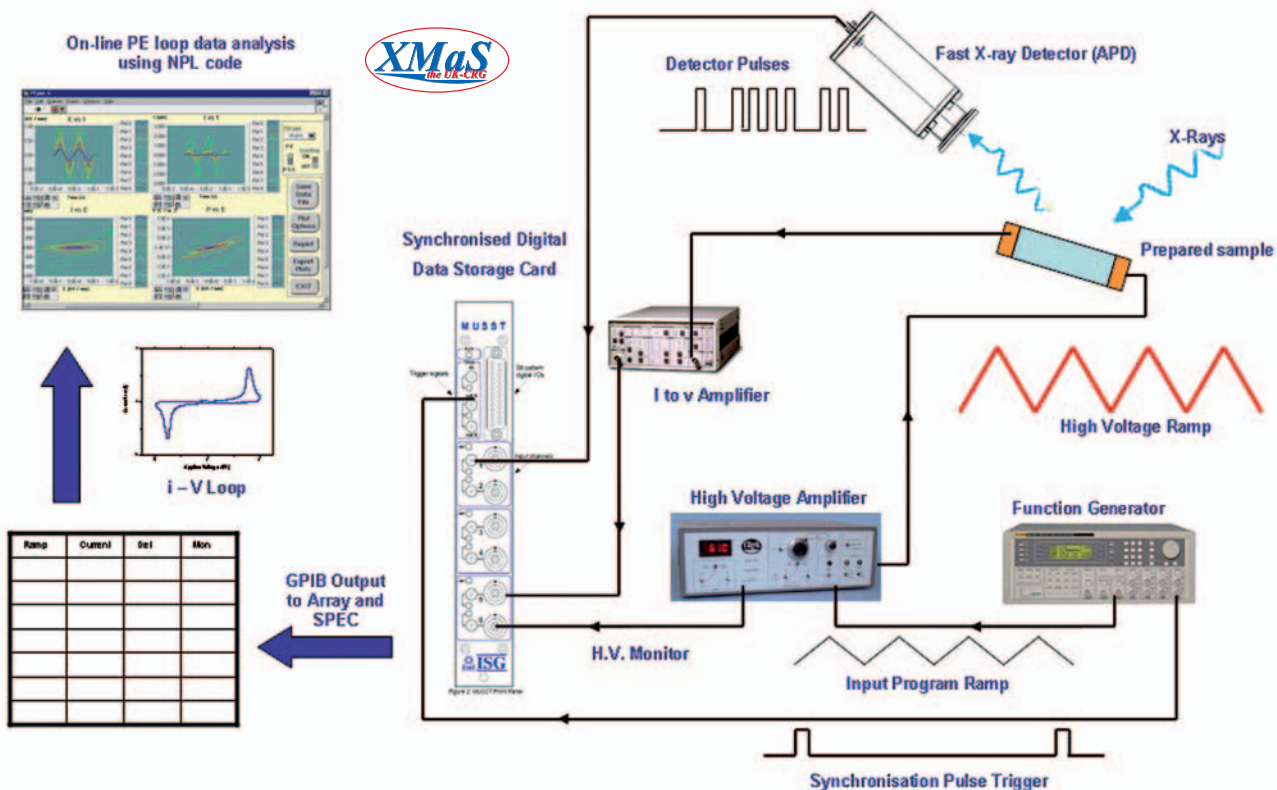


Figure 3: Schematic of in-situ P-E loop measurement system at XMaS

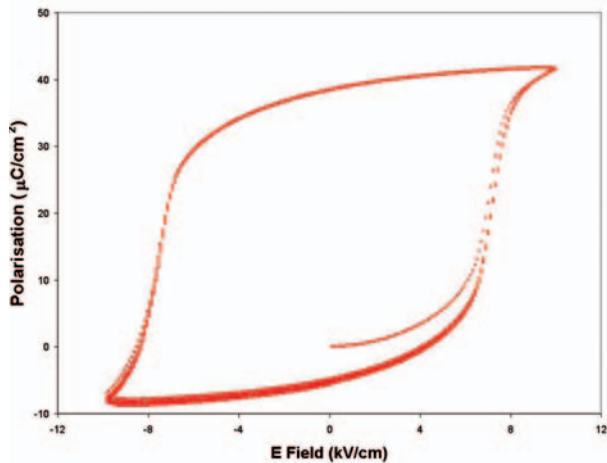


Figure 4: Polarisation Field (P-E) measurement of poled soft PZT composition taken at 1 Hz, five consecutive loops overlaid.

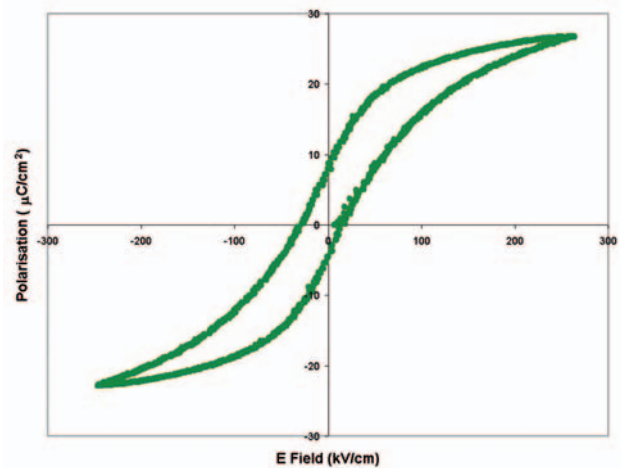


Figure 5: Polarisation Field (P-E) measurement of a 1 μF ceramic multilayer capacitor taken at 1 Hz. The sample is a composite multiferroic with a sandwich of piezoelectric dielectric with magnetostrictive nickel electrodes.

Fluorescence yield XMCD

The XMaS team has been developing a setup to facilitate measurements of reflectivity and X-ray Magnetic Circular Dichroism (XMCD) signals simultaneously under identical experimental conditions. Fluorescence yield is generally the mode adopted to collect XMCD spectra as sample thickness is often the limiting factor for transmission measurements.

Here we describe the advances made with measuring XMCD signals using a 5 μm thick Gd polycrystalline foil as a test sample. The fluorescence was measured with a photodiode mounted directly inside the shroud of the cryostat. The diamond flipper was used to reverse the helicity of the x-ray beam produced by the 0.8 mm thick diamond phase-plate at 11.5 Hz for each energy across the Gd L_2 edge. Each spectrum (Figure 6) represents the “half-difference” between data collected for opposite magnetic field directions. This eliminates non-magnetic effects which add noise and background signals to the spectral fine structure. The dichroic (lines with dots) and absorption (solid line) spectra were collected simultaneously with a lock-in amplifier (blue lines) and the MUSST fast acquisition card (red lines), for comparison.

The spectra obtained numerically with the MUSST have a better quality than those measured with the analogue lock-in. Unlike the lock-in, the digital method also records information for each helicity individually. Furthermore, a delay time can be adjusted within the card so that data are only collected when the flipper reaches the position for which the degree of circular polarization is a maximum. Thus this method is demonstrably superior.

The fluorescence yield technique needs now to be applied in conjunction with reflectivity for experiments at low energies (see for example the study of Pd

moments in this Newsletter) where beam attenuation must be minimised. A photodiode array has been designed to fit inside the in-vacuum electromagnet chamber for fluorescence detection in backscattering geometry. A windowless avalanche photodiode will also be available for the reflectivity measurements over a large dynamic range. A cryostat also fits inside the chamber. The whole setup eliminates the use of kapton windows and beryllium shrouds. Measurements of electron drain currents are also envisaged. Finally, great care will have to be taken to eradicate the source of noise present in the reported spectra.

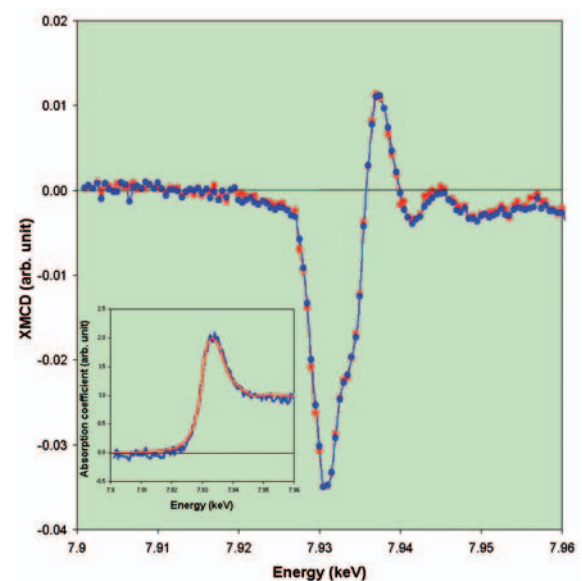


Figure 6: Fluorescence yield XMCD and absorption coefficient (inset) measured at 112 K with the lock-in (blue) and the MUSST card (red) for comparison.

Probing the crystal field of spin-orbital-lattice coupled SmVO_3

R. D. Johnson, S. R. Bland, T. A. W. Beale, P. D. Hatton, L. Bouchenoire, D. Prabhakaran, A. T. Boothroyd – For further information contact R. D. Johnson, Department of Physics, University of Durham, UK

r.d.johnson@durham.ac.uk

Recent advances have uncovered strong interaction between spin, orbital and charge degrees of freedom within single crystals. These microscopic properties, closely coupled to the crystal lattice, are particularly pronounced in transition metal oxides. In some materials it has even been shown that it is possible to manipulate the electronic correlations by the control of external parameters such as electric and magnetic fields. The understanding of ordering phenomena in these systems is therefore of great technological and fundamental scientific interest.

The RVO_3 series (R = rare-earth ion or yttrium) has attracted continuous study as they form a set of materials in which the vanadium t_{2g} orbital, spin and lattice degrees of freedom are closely coupled [1]. In SmVO_3 , the room temperature orthorhombic crystal undergoes a transition to a monoclinic structure at 193 K. This occurs simultaneously with the onset of a G-type orbital order. On further cooling, C-type magnetic order develops below 130 K.

Here we report on recent resonant x-ray scattering (RXS) results, performed on XMaS of the (011) anisotropic tensor of susceptibility (ATS) reflection. This was measured in the room temperature and the low temperature orbital and magnetic ordered phases of SmVO_3 . The crystal field of the vanadium ions was probed by measuring the resonant enhancement of the ATS reflection that exists at the vanadium K-edge, as a function of energy. The energy spectra were then compared to predictions made by the *ab-initio* FDMNES code.

Figure 7a shows the RXS energy spectra observed. We note that there is no significant difference between 105 K and 165 K, except for a slight decrease in intensity. Therefore, the magnetic order occurring at 130 K would appear to have no effect on the crystal field of the vanadium ions. We do, however, observe a subtle change in lineshape, as well as a dramatic reduction in intensity, when comparing the 165 K spectra to that measured at 293 K. We suggest this is a consequence of the small monoclinic distortion, occurring at 193 K, along with a reduction in intensity due to thermal effects. To exclude the possibility of contamination from other scattering processes, we simulated the spectra using the FDMNES code [2]. In the calculation we consider only the crystal structure without invoking any other electronic order. The excellent agreement of experiment with the calculation (Figure 7b) demonstrated that the diffraction signal is primarily sensitive to the crystal field. ■

[1] S. Miyasaka, et al., Phys. Rev. B 68, 100406 (2003).

[2] Y. Joly, Phys. Rev. B 63, 125120 (2001).

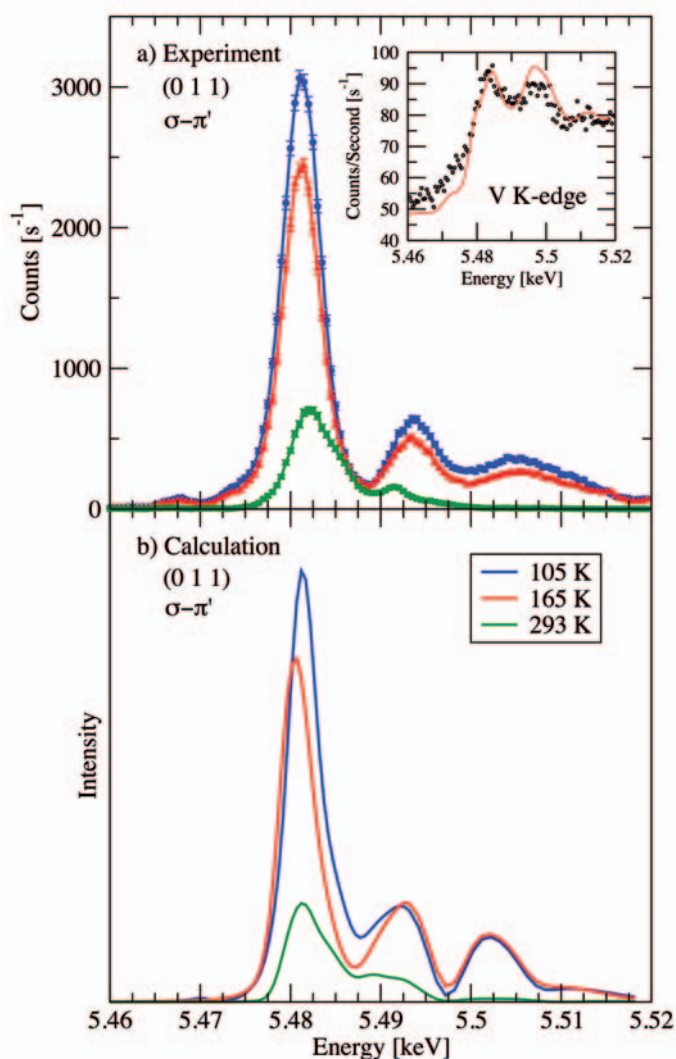


Figure 7: a) RXS energy spectra of the (011) ATS reflection measured through the vanadium K-edge. The inset shows the fluorescence spectrum (black) and its calculation (red). b) Energy spectra calculated by employing the FDMNES code.



3D Ordered Gold Strings by Coating Nanoparticles with Mesogens

X. B. Zeng, F. Liu, G. Ungar, A. G. Fowler, L. Cseh, G. H. Mehl, and J. E. Macdonald – For further information contact X. B. Zeng, Department of Engineering Materials, University of Sheffield, UK
X.Zeng@sheffield.ac.uk

Metallic nanoparticles have attracted great interest for their potential electronic, optical, photonic and medical applications. These applications normally require the fabrication of bulk 3-d arrays of metal nanoparticles, or "meta-atoms", with prescribed geometrical layouts. So far most of these arrays could only be produced with exceptionally uniform nanoparticles, and the range of array types was limited by the particle shape e.g. cubic arrays from spherical particles. Recently Georg Mehl and Liliana Cseh of Hull University attempted to change this situation by grafting liquid crystal molecules side-on to the nanoparticles [1]. In a recent collaboration between research groups from Sheffield, Hull and Cardiff Universities, self-assembled 3-d and 2-d arrays of these LC-coated gold nanoparticles were reported [2].

Two different mesogen-covered gold nanoparticle systems were studied (Figure 8). Small nanoparticles (ca. 2 nm in diameter) were used. Such materials preserve the ability of the mesogens to form a liquid crystalline phase. The alignment of the mesogens breaks the cubic symmetry that the nanoparticles would normally adopt, and introduces anisotropy to the periodic lattices that form.

Grazing Incidence Small Angle X-ray Scattering (GISAXS) patterns from well-oriented films of systems 1 and 2, prepared on silicon substrate (Figure 9)

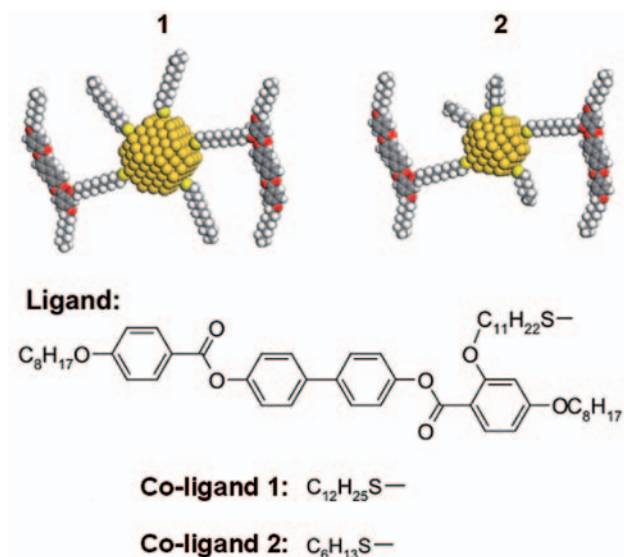


Figure 8: Schematic structure of the gold nanoparticles coated with mesogens and alkythiols.

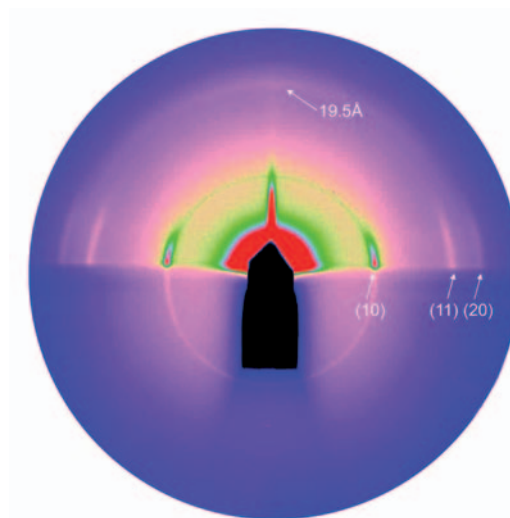
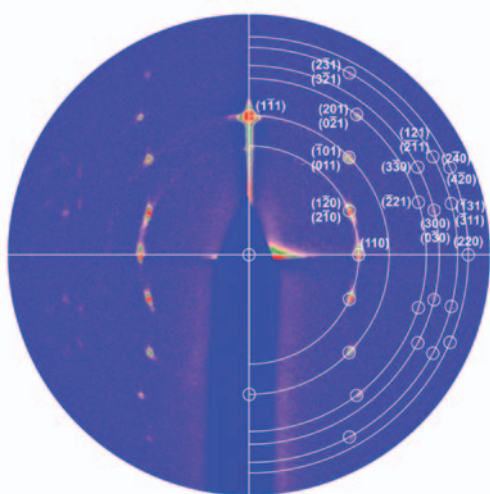


Figure 9: GISAXS diffraction patterns of system 1 (left) and 2 (right).

were found to be extremely useful in determining the structures of these anisotropic arrays. From these patterns, 1 was found to form a 3-d rhombohedral lattice with space group $R\bar{3}m$, while 2 was shown to organise into a 2-d hexagonal columnar lattice. The schematic models of the two phases are shown in **Figure 10**.

GISAXS experiments on oriented films of 2 provided additional information about the columnar phases. **Figure 9 (right)** shows that the nanoparticle columns stand perpendicular to the substrate surface. A weak diffuse meridional scattering peak indicates that the average distance between neighbouring gold nanoparticles within a column is just 2.0 nm.

The mesophase structure of both 1 and 2 can be described as consisting of strings of nanoparticles surrounded by a sheath of axially aligned mesogens. A significant feature illustrated by the present results is the remarkable scope for varying the interparticle distance in the column direction simply by varying the length of the co-ligand thioalkyl chains. Thus, while in 1 the interparticle gap is 1.7 nm, in 2 the gap virtually disappears and the nanoparticles touch in the direction of the string.

This work demonstrates that highly ordered superlattices of metal nanoparticles other than those expected from mere packing of spheres can be created by coating the particles with liquid crystals. The results establish the first rules on which to base future design of more complex lattices with a view to build self-assembled metamaterials. ■

- [1] L. Cseh, G. H. Mehl, *J. Mater. Chem.* 17, 311 (2007).
 [2] X. B Zeng et al., *Adv. Mat.* 21, 1746 (2009).
 [2] J.M. Effantin et al., *J. Magn. Magn. Mater.* 47-48, 145 (1985).
 [3] S. Kobayashi et al., *J. Phys. Soc. Jpn* 70, 1721 (2001).
 [4] H. Walker et al., *Phys Rev B* 79, 054402 (2009).

X-ray resonant scattering study of the structural and magnetic transitions in PrB_6

H. C. Walker, K. A. McEwen, D. F. McMorrow, M. Bleckmann, J.-G. Park, S. Lee, F. Iga, D. Mannix –
 For more information contact H. Walker, European Synchrotron Radiation Facility, France.

helen.walker@esrf.fr

The RB_6 compounds have attracted significant theoretical and experimental attention in recent years as they show a variety of interesting electronic and magnetic properties, and their simple cubic $\text{Pm}\bar{3}m$ crystal structure makes them attractive model systems for the study of multipolar order and its role in the magnetic and electrical properties of f electron systems. PrB_6 exhibits two magnetic phase transitions: (i) at $T_{N1}=7$ K to an incommensurate (IC) antiferromagnetic (AFM) phase and (ii) at $T_{N2} = 4.5$ K to a commensurate (C) AFM phase. Neutron diffraction results [1] have been interpreted in terms of a planar $2k$ magnetic structure, which in the commensurate phase is reminiscent of the phase III structure of CeB_6 [2]. This structural commonality combined with a reduced ordered moment of $1.2\mu_B/\text{Pr}$ ion, as opposed to the expected $2.0\mu_B/\text{Pr}$ ion, suggests competition between antiferromagnetic and quadrupolar exchange interactions [3], and motivated our study into the magnetic structure and search for quadrupolar order [4].

At the beginning of our experiment, it immediately became apparent that the superior wave-vector resolution at XMaS provided evidence of a structural distortion at low temperatures. Mesh scans of reciprocal space close to the (222) reflection revealed a splitting of the one peak at 5.5 K into four peaks at

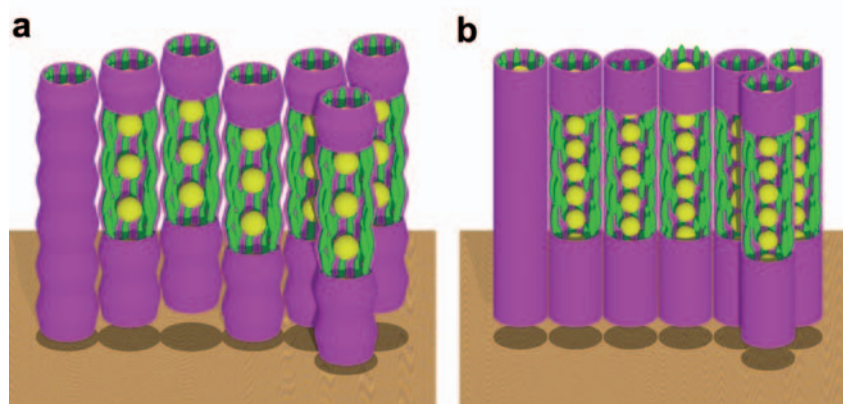


Figure 10: Schematic models of the (a) rhombohedral phase in system 1 (b) the hexagonal columnar phase in system 2; yellow: gold nanoparticles, green: mesogens.



1.8 K (see Figure 11), consistent with a rhombohedral distortion. Tracking the temperature dependence of the peak splitting demonstrated that the structural transition is concomitant with the C-IC magnetic transition at T_{N2} . The magnetic dependence of the structural distortion was also investigated, and it was found that in small applied fields the split peaks move to higher values of h, k, l indicating a negative magnetostriction. For larger applied magnetic fields the peak splitting was suppressed.

The magnetic structures were investigated in both AFM phases using resonant scattering. Satellite reflections were observed and displayed energy resonances. Second harmonic satellites were also observed arising from charge ordering, reminiscent of the secondary lattice distortion associated with the AFM order in isostructural GdB6. In the commensurate phase the azimuthal dependence of the magnetic scattering was measured (Figure 12) and found to be consistent with the model of Burlet deduced from neutron diffraction.

The antiferroquadrupolar propagation vector in CeB₆ is $(1/2 \ 1/2 \ 1/2)$ [2], and we have found an analogous superlattice peak in PrB₆ at $(1/2, 3/2 \ 3/2)$, which could indicate quadrupolar order. However these measurements were performed at the E1 resonance energy, such that we were probing the 5d electrons rather than the 4f electrons which would give rise to the proposed electric quadrupole moments. Therefore to provide a direct observation of the

ordering of the 4f quadrupole moments, we plan further measurements to investigate the temperature and azimuthal dependences of this superlattice reflection, at the E2 transition energy. ■

- [1] P. Burlet et al., J. Phys. (Paris) 49, C8 (1988).
- [2] J.M. Effantin et al., J. Magn. Magn. Mater. 47-48, 145 (1985).
- [3] S. Kobayashi et al., J. Phys. Soc. Jpn 70, 1721 (2001).
- [4] H. Walker et al., Phys Rev B 79, 054402 (2009).

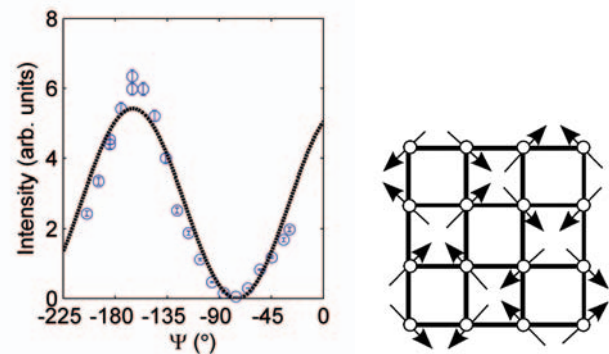


Figure 12: Azimuthal dependence of resonant scattering from the $(1/2, 5/4, 5/4)$ commensurate magnetic reflection with calculation for the structure shown to the side.

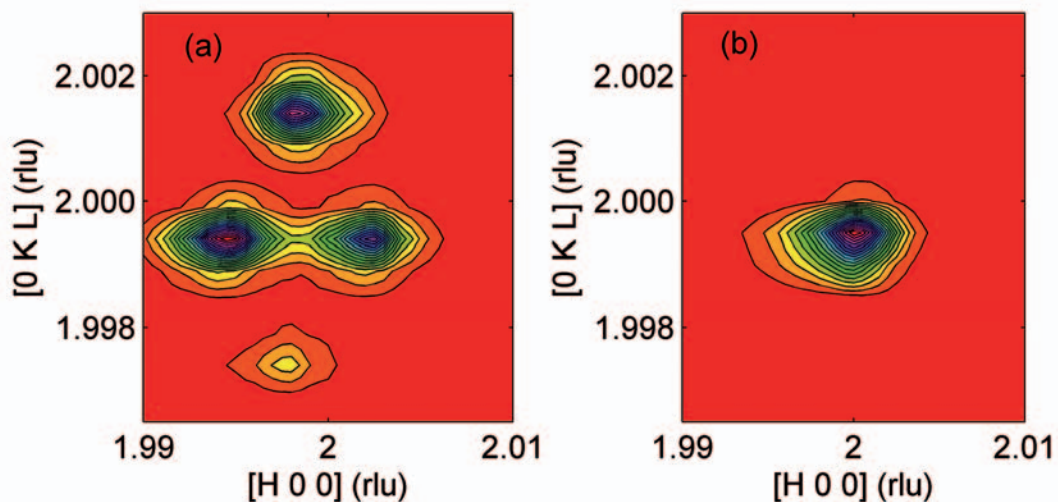


Figure 11: Reciprocal space mesh scans around (222) Bragg peak at (a) $T=1.8$ K and (b) $T=5.5$ K.

Study of Pd moments using circularly polarised x-rays

T.P.A. Hase, L. Bouchenoire, P. Thompson, S. Brown, P. Normile and B. Hjorvarsson - For further information contact T.P.A. Hase, Department of Physics, University of Warwick, UK

T.P.A.Hase@warwick.ac.uk

We present magnetic scattering from a $[\text{Fe}(2\text{ML})\text{Pd}(15\text{ML})]_{\times 20}$ multilayer grown using ultra high vacuum sputtering on a 20nm Pd buffered (100) MgO substrate at the University of Uppsala. Due to its high magnetic susceptibility paramagnetic Pd is easily polarised by the presence of a transition metal ferromagnet such as Fe [1]. In these multilayers a significant percentage of the total magnetic moment is carried by an induced moment on the Pd.

Room temperature resonant reflectivity was measured at the Pd L3 edge (3.17 keV) using circularly polarised x-rays produced by a 100 μm diamond phase-plate. The sample was mounted using the in-vacuum magnet which applied fields in the scattering plane. Although XMaS is not yet fully optimised for such soft x-ray energies, it was still possible to record high quality reflectivity data over a dynamic range of seven orders of magnitude with a counting time of five seconds using a fixed helicity (Figure 13): in the inset a clear difference between data recorded with opposite applied fields was seen

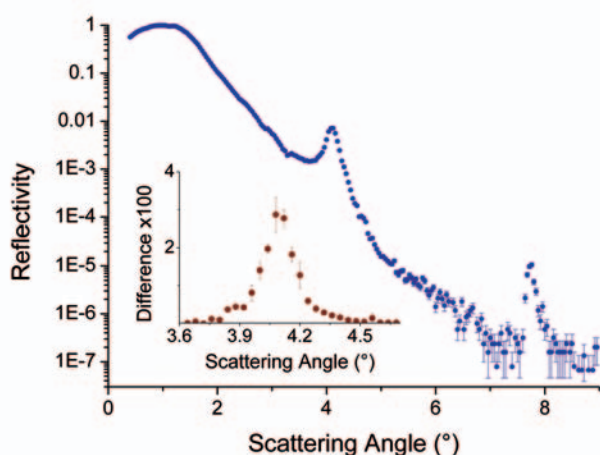


Figure 13: Field averaged reflectivity recorded with a fixed positive helicity. A clear difference between field directions was observed at the first Bragg Peak (inset).

at the first Bragg peak indicating significant polarisation of the Pd layers [2].

In Figure 14 we show how the Bragg peak intensity varies as a function of energy. The sum data are identical when the incident helicity is reversed and shows characteristic fine structure oscillations above the absorption edge. In contrast, the difference signal is clearly a resonant feature which changes sign on reversal of the incident helicity.

The field dependent behaviour of the induced Pd moment can be extracted by measuring the Bragg peak intensity as a function of applied field (Figure 15). A square ferromagnetic response is observed with a coercive field of 5.0 ± 0.5 mT, in excellent agreement with other bulk magnetic probes.

XMaS is currently unique in Europe in providing direct user access for 4d resonant scattering studies. A further advantage of XMaS is the ability to reverse the helicity rapidly by means of the diamond flipper. Although excellent data can be obtained in the current configuration, we expect a substantial increase in the signal-to-noise arising from the increase in flux following instrumental developments described elsewhere in this Newsletter. As well as enhancing the signal-to-noise levels, remnant magnetic studies will be possible. ■

[1] J. Crangle, Phil. Mag. 5, 335 (1960).

[2] S. Brown et al., Phys. Rev. B. 77, 014427 (2008).

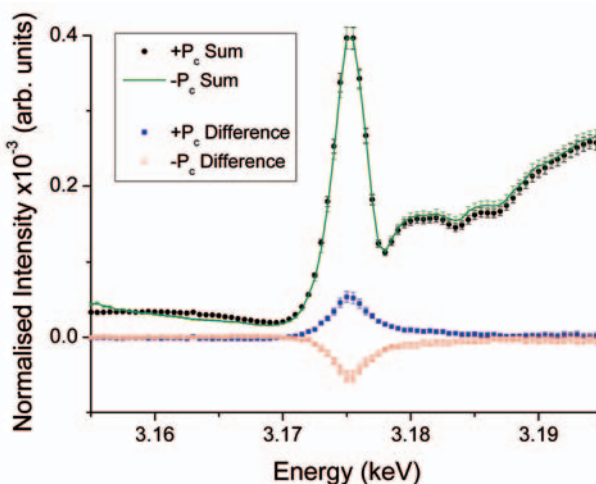


Figure 14: Energy dependence of the sum (top curves) and difference (bottom curves) signals for both helicities.



Resonant Borrmann Effect in Rutile

M. Tolkiehn, S. P. Collins – For more information contact M. Tolkiehn, HASYLAB at DESY, Hamburg, Germany.

martin.tolkiehn@desy.de

The Borrmann effect is one of the most remarkable manifestations of dynamical X-ray diffraction. It describes a dramatic increase in transparency to X-ray beams at certain Laue reflections. While the reduction of dipole absorption, caused by the standing wave field in the crystal, was discovered [1] and described theoretically [2] already half a century ago, it has only been discovered recently by Pettifer *et al.* [3] that quadrupole absorption is dramatically enhanced in the Borrmann effect. For certain reflections the low electrical field intensity at the atoms leads to a low dipole absorption (anomalous transmission). At the same time the high field gradient results in an enhanced quadrupole absorption. Therefore the intensity of the diffracted beam strongly depends on the quadrupole absorption cross section of the atoms at the nodes of the standing wave field. This was demonstrated for quadrupole transitions observed in the X-ray absorption near edge structure (XANES) of the Gd L-edges in Gadolinium Gallium Garnet (GGG).

In a recent experiment at the XMaS beamline we used this effect to investigate quadrupole features in the Ti K-edge XANES in rutile (TiO_2). The integrated intensity of the (020) reflection was measured at different energies around the Ti K-edge and compared to Ti K fluorescence measured at large deviations from the Bragg scattering conditions. The absorption spectra obtained from both signals are shown in **Figure 16**. While there are three pre-edge peaks clearly visible in the Borrmann signal (red line), the first peak (A) is hardly visible in the conventional spectrum (blue line) obtained from the fluorescence signal. This clearly identifies peak A as a quadrupole transition. Peaks B and C, which have the same height in the conventional spectrum, are also enhanced in the Borrmann signal, where B is stronger than C. This could mean that B and C are dipole peaks with a certain quadrupole contribution, which is stronger for peak B. Most probably C is a pure dipole peak and B is a mixed dipole quadrupole peak. These results are in a good agreement with the results by Uozumi *et al.* [4].

Results from the (002) and (110) reflections give a more modest enhancement, which also supports the same conclusions regarding the multipole origin of these pre-edge peaks. The reason for the much larger enhancement at the (020) Laue reflection is currently being investigated.

Our results show that the resonant Borrmann effect is a well suited tool for the investigation of the nature of

pre-edge peaks in XANES spectra. This new technique is very promising for the investigation of 3d states at transition metal K-edges and 4f states at rare earth L-edges, both of which play an important role in electronic and magnetic properties. ■

- [1] G. Borrmann, Physikal. Zeit. 42, 157 (1941).
- [2] M. von Laue, Röntgenstrahlinterferenzen, Akademische Verlagsgesellschaft, Frankfurt am Main (1960).
- [3] R. F. Pettifer, S. P. Collins, D. Laundry, Nature 454, 196 (2008).
- [4] T. Uozumi, K. Okada, A. Kotani *et al.*, Europhys. Lett. 18, 85 (1992).

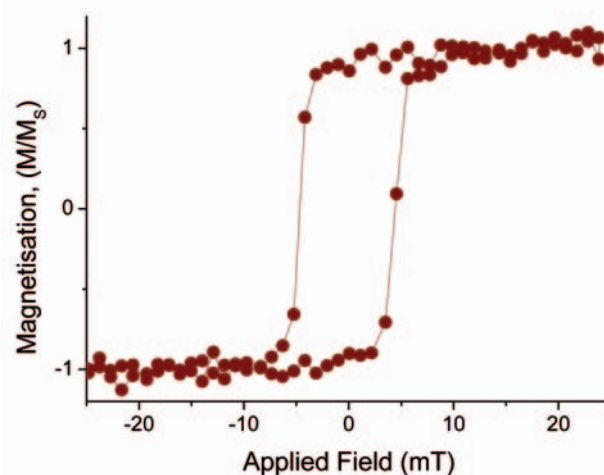


Figure 15: Induced Pd moment recorded as a function of applied field with a fixed incident helicity. The coercive field is 5.0 ± 0.5 mT.

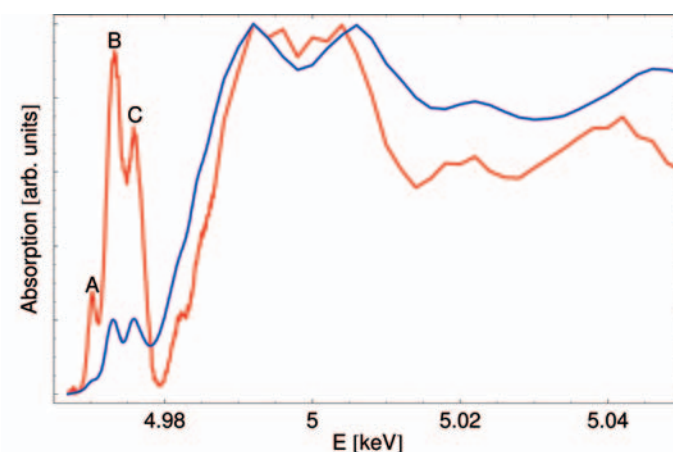


Figure 16: Absorption of TiO_2 at the Ti K-edge determined from Ti-K fluorescence yield (blue line) and from the integrated intensity of the (020) Laue reflection (red line).

XEOL for microscopy on XMaS

M. Dowsett and A. Adriaens - For further information contact M. Dowsett, Department of Physics, University of Warwick, UK

m.g.dowsett@warwick.ac.uk

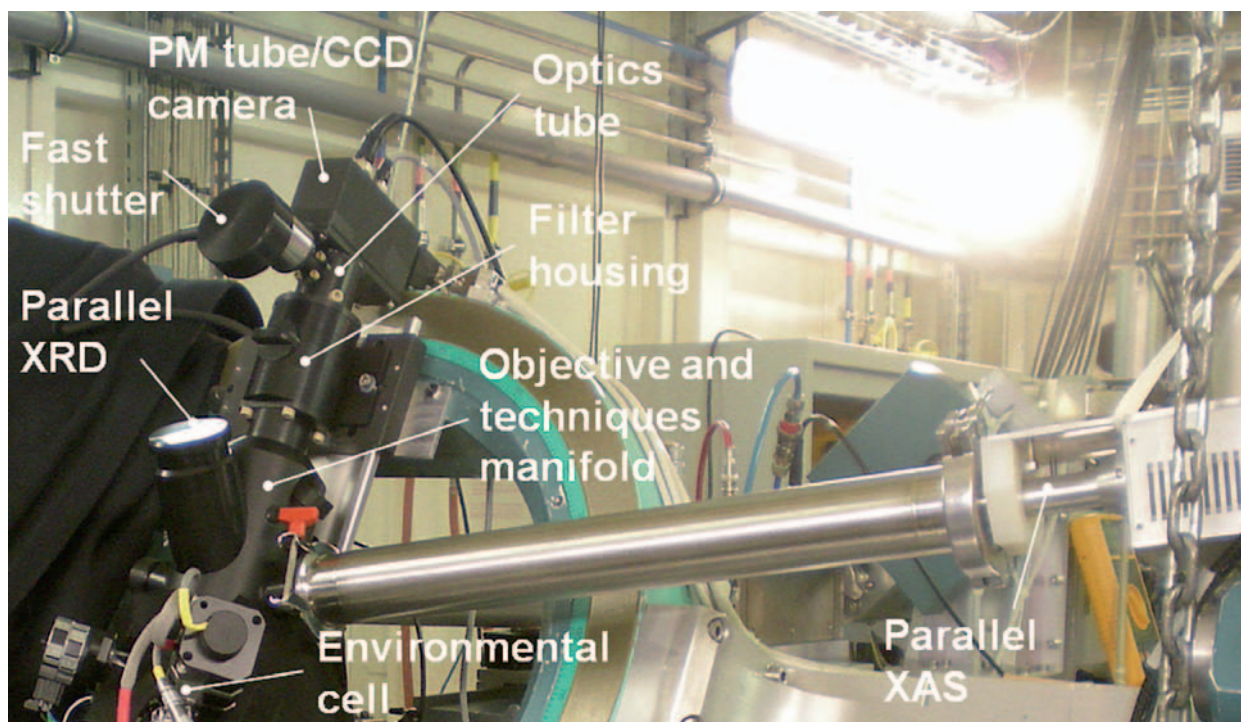
Bombardment of materials by keV X-rays results in broadband (200 - 1000 nm) transoptical emission due to fluorescence and phosphorescence – X-ray excited optical luminescence (XEOL). In particular, when the X-ray energy is swept across core ionization energies of the atoms, the processes which impose XANES and EXAFS modulation on the fluorescent X-ray emission, also modulate the optical wavelengths, sometimes in a near-identical fashion. Other related processes, for example the production of low energy photoelectrons generated by core level ionization close to the edge energy, can excite narrow-band optical transitions within 10-100 nm [1] of the ionized atom. The transoptical emission is therefore a rich potential source of information about the electronic state and local structure of the surface. Moreover, since the escape depths of the photons concerned are typically much less than those of the accompanying X-ray fluorescence, the information is more surface specific. A combination of broadband light-optical imaging combined with filtering or dispersion therefore forms the basis for a spectromicroscopy which has the potential to give both site and state specific information. Indeed, a microscopy system (MOLES) based on this principle was developed by Poolton *et al.* [2] at SRS Daresbury, and the technique has also been

developed at ESRF (on ID22) by Martínez-Criado [3], this time using an X-ray microprobe. However, because XEOL can give chemical imaging with micron-scale lateral resolution, without the need for a microfocus beam-line, it is ideally suited to beam lines such as XMaS with reasonably large beam footprints, but also high flux. Whole images and spectra can be captured by a CCD camera without the need to scan the beam, and therefore the speed of image acquisition is controlled directly by the statistical precision required. This may be as little as a few seconds in some cases.

Our interest in the technique lies in its potential for surface imaging of chemical processes occurring in real time inside an environmental cell, for example in heritage metals research. As part of ESRF LTP EC188 we have constructed a proof of concept optical system (Figure 17) with which we can collect conventional X-ray fluorescence for XAS measurements in parallel with XEOL. Results for copper and zinc K edges and the lead L₃ edge show that XEOL-XAS can detect thin layers on surfaces, revealing the presence of corrosion layers invisible to conventional XAS where the layer signal is swamped by that of the substrate [4,5].

Figure 18 demonstrates this surface specificity for a thin nantokite (CuCl) layer on copper. In the conventional XAS data (black curve) only the copper XANES and EXAFS structure is detectable (cf the red curve for pure copper). Conversely, the XEOL-XAS spectrum (green curve) is dominated by the CuCl emission. In addition, colour filtering of this spectrum shows that while most of the spectrum is due to

Figure 17: Setup for XEOL measurements.



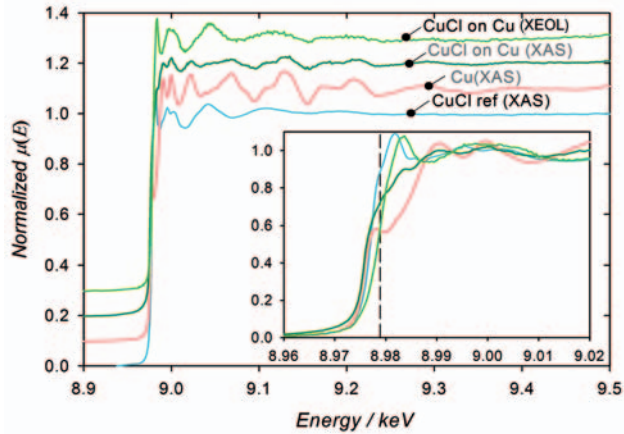


Figure 18: Demonstrating the surface specificity of XEOL for a thin nantokite layer on copper. Spectra are offset in intensity for clarity in the main figure. The inset shows the edge region with no offset in more detail.

broadband optical emission, the so-called white line structure at the edge is restricted to green photons. In similar experiments, it should be possible to identify the radiative transitions responsible for near edge structures unambiguously from the optical spectroscopy. Based on this work, we have been awarded funding for the construction of a full-scale CCD based spectromicroscope which will be developed on XMaS and DUBBLE. ■

- [1] D. A. Hill et al., J. de Physique IV 7, 553 (1997).
- [2] N.R.J. Poolton et al., Nucl. Instrum. Meth. B 246, 445 (2006).
- [3] G. Martinez-Criado et al., Appl. Phys. Lett. 89, 221913 (2006).
- [4] M.G. Dowsett et al., Anal. Chem. 80, 8717 (2008).
- [5] <http://www2.warwick.ac.uk/fac/sci/physics/research/condensed-matt/SIMS/>

Engineering the charge-density wave ground state in uranium thin films

J. Chivall, R. Springell, P. Normile, B. Detlefs, R. C. C. Ward, and G. H. Lander – for further information contact J. Chivall at University College London, UK.
j.chivall@ucl.ac.uk

Charge density wave (CDW) ordering is an intriguing phenomenon which is coming under increasing focus due to its potential role in high-temperature superconductivity [1]. Bulk α -uranium (orthorhombic structure) exhibits CDW order below a temperature, T_{CDW} , of 43 K, where a lattice relaxation also takes place (an effect related to the CDW formation) [2]. Initially the CDW order is incommensurate with the underlying crystal lattice – its wavevector $(q_a, q_b, q_c) = (0.5, \sim 1/6, \sim 2/11)$ reciprocal lattice units, where a, b, and c denote the orthorhombic crystal axes – however, in bulk α -U, as the temperature is lowered all three wavevector components lock-in to commensurate values.

Being a single element system exhibiting a conveniently high T_{CDW} , uranium is an ideal case in which to study CDW ordering. Following on from earlier work [3], our interest in these XMaS experiments is in the use of epitaxial growth of thin-film U as an avenue by which to explore CDW behaviour. Specifically, we investigate here the effect of U layer thickness on the CDW transition, by studying x-ray diffraction from α -U films grown on (1,1,-2,0) sapphire substrates with Nb buffer and capping layers. Figure 19 shows a reciprocal space map in the (2.5, K, L) plane for a 1000 Å sample, where a total of four CDW satellite reflections – two strong and two weak – are observed positioned about a weak signal at the (2.5, 2, 1) position. (In each film studied here, the [110] direction is parallel to the sample surface normal.) In bulk α -U, these four satellite intensities are within 50% of one another, whereas in Figure 19 large (~ more than an order of magnitude) intensity variation is found in the $(q_a, \pm q_b, q_c)$ satellite pairs. We find such strong $\pm q_b$ asymmetry to be a general feature over the U thickness range of these studies. Furthermore, in contrast to bulk α -U, no commensurate lock-in transitions are observed; q_b tends to its bulk value upon reducing temperature, but q_c is temperature independent.

Figure 20 shows a comparison of the integrated intensities of scans taken along the [001] (in plane) direction through the two most intense CDW satellite positions (Figure 19) and through the (221) Bragg peak, as a function of U film thickness. The decrease in intensity is linear as expected for the (221) peak, whereas the satellite intensity appears to fall-off more rapidly at low thickness. Sample rocking curves of

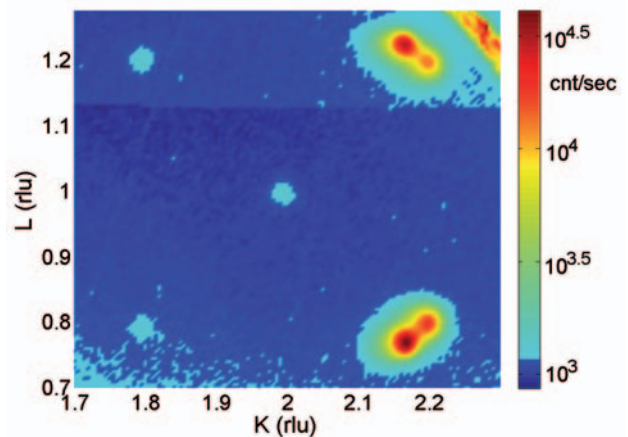


Figure 19: (2.5, K, L) reciprocal space map for a 1000 Å U film recorded at 10 K using 8.5 keV x-rays. Two strong (upper and lower right corners) and two weak (upper and lower left corners) CDW satellites are observed, as well as a weak peak at (2.5, 2, 1). The strong (positive q_b) satellites appear as doublets because each one is in near coincidence with a higher order satellite. A segment of a Debye-Scherrer cone from the beryllium domes of the cryostat also appears in the upper right corner. (All intensities have been monitor corrected.)

the specular (110) Bragg reflection show a two-component lineshape: a narrow, pseudomorphic, Gaussian and a “relaxed” component with a Lorentzian-squared form. The inset in **Figure 20** shows the situation for the thinner films, where the pseudomorphic component becomes most pronounced. A plausible scenario, which could account for the more rapid fall-off in satellite intensity at low U thickness, is that in the volume of a film associated with its pseudomorphic component, the lattice degrees of freedom are constrained such that the CDW does *not* form. ■

- [1] S. Kivelson et al., Rev. Mod. Phys. 75, (2003).
 [2] G. H. Lander et al., Advances in Physics 43, (1994).
 [3] R. Springell et al., Phys. Rev. B 78, 193403 (2008).

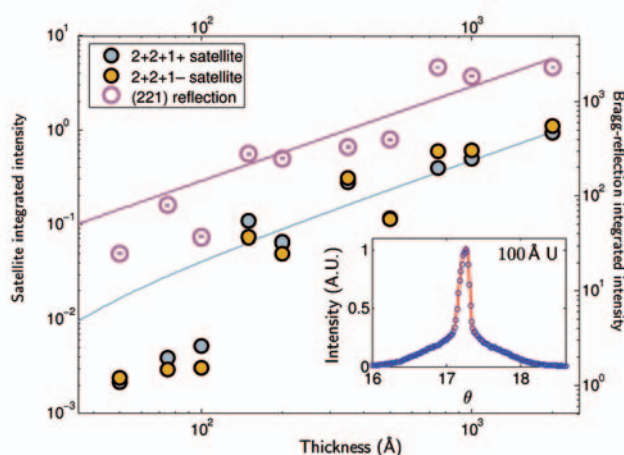


Figure 20: Integrated intensity of the CDW satellites and the (221) Bragg reflection as a function of U thickness. The solid lines are linear trends (see text). Inset: representative rocking curve of the (110) reflection in thinner films. The figure demonstrates the existence of the CDW down to the lowest U thickness studied (50 Å).

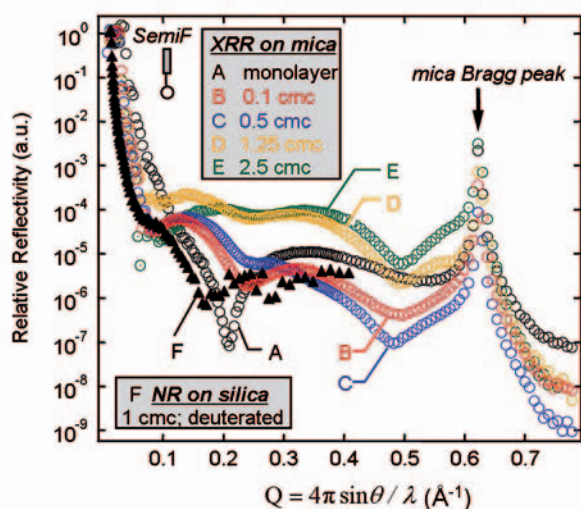


Figure 21: XRR of a SemiF surfactant on mica in air (A circles) and in solutions (B-E circles), obtained at XMaS. Comparison with neutron reflection (NR) on silica in 1 cmc deuterated SemiF D_2O solution (F triangles) obtained at ISIS by R. Thomas (Oxford).

Adsorption of Surfactants at Mica-Water Interface

W.H. Briscoe, R.J. Jacobs, F. Speranza, P. Li, J. Klein, R.K. Thomas and L. Bouchenoire - For further information contact W.H. Briscoe, School of Chemistry, University of Bristol, UK

wuge.briscoe@bristol.ac.uk

The surfactant adsorption process at the solid-liquid interface is of great importance in many fields, such as wettability control, detergency, surface nano-patterning, mineral flotation, nanofluidics and boundary lubrication. Much of our understanding of this process derives from hydrocarbon surfactants (H-*surf*; hydrogenated) on model substrates such as silica and silicon, using techniques such as AFM, ellipsometry and neutron reflectometry. For instance, AFM imaging has revealed that H-*surf* could form discrete surface aggregates of different morphologies including (patchy) monolayers and bilayers, surface micelles or hemi-micelles, and hemi-, flattened or full cylinders. The outcome depends intricately on bulk solution conditions such as pH, surfactant and electrolyte concentrations, the type of the counterions to surfactant headgroups, and particularly, the molecular architecture of surfactants and the nature of solid substrates – the electric charge density, functional groups and hydrophobicity.

An effective way of controlling the surfactant architecture is to incorporate fluorinated segments in the surfactant molecule, resulting in hydrocarbon-fluorocarbon hybrid surfactants, *i.e.* semi-fluorinated surfactants (SemiF) which are reported to exhibit aggregation behaviour in the bulk that depend on their degree of fluorination and the location of fluorinated segments in the SemiF molecule.

Using a homemade liquid cell and a novel “bent mica” method [1] on XMaS, we have made the first studies of the structures of twenty different H-*surf* and SemiF surfactants at the mica-water interface using X-ray reflectometry (XRR) – see **Figure 21**. The analysis (still in progress) of the XRR Kiessig fringes shows a gradual build-up of the layer thickness and coverage as the bulk SemiF surfactant concentration increases. In particular, we note that the XRR Kiessig fringes are more pronounced than those from neutron reflectivity (▲ in **Figure 21**). This indicates the suitability of XRR as a general technique for examining surfactant structures at mica surfaces. Such structural information is inaccessible by other optical reflectance techniques due to mica’s birefringence and thus XRR is invaluable to a number of force measurement techniques where mica is routinely used as a model substrate [2]. ■

- [1] W. H. Briscoe et al., J Colloid Interface Sci 306, 459 (2007).
 [2] M. Chen et al., Science 323, 1698 (2009).



Magnetic order in a new multiferroic, samarium-based manganite

D. O'Flynn, G. Balakrishnan, M. R. Lees, J. S. Gardner, P. Normile and C. Giles – for further information contact D. O'Flynn, Department of Physics, University of Warwick, UK.

d.oflynn@warwick.ac.uk

Research in the field of multiferroics has intensified since the discovery in 2003 of a novel class of materials, the so called “type-II” multiferroics, in which the nature of the magnetic order causes ferroelectricity [1]. Up to now Resonant X-ray Scattering (RXS) has been employed in this field of research perhaps most notably to study the archetypal type-II multiferroic TbMnO_3 , where it has served as a complementary probe to neutron diffraction [2]. However, when manganites are formed with rare earths which, in their naturally occurring isotopic forms, are strongly neutron absorbing isotopes (e.g. Sm or Gd), RXS can be the most convenient method to solve the full details of the magnetic structure, beginning with the determination of the magnetic wavevector(s) and domains, a task usually undertaken with neutrons.

Here we report results from our recent XMaS experiment on $\text{Sm}_{0.5}\text{Y}_{0.5}\text{MnO}_3$, a concentration from the $\text{Sm}_{1-x}\text{Y}_x\text{MnO}_3$ family we have recently found (from bulk studies) to be multiferroic [3]. Like TbMnO_3 , the multiferroic state appearing in $\text{Sm}_{0.5}\text{Y}_{0.5}\text{MnO}_3$ is signalled by a second antiferromagnetic phase transition seen in magnetization measurements. The temperature for the transition, $T_{N2} \approx 20$ K, is some 7 K below T_{N2} in TbMnO_3 [1, 2]. In fact, it is the onset of a *cycloidal* antiferromagnetic phase at T_{N2} in TbMnO_3 which is responsible for the ferroelectricity [1]. Confirmation that such a phase occurs in $\text{Sm}_{0.5}\text{Y}_{0.5}\text{MnO}_3$ was beyond the scope of the present experiment, where the aim has been simply to determine the wavevector and domains present in $\text{Sm}_{0.5}\text{Y}_{0.5}\text{MnO}_3$ in its $T < T_{N2}$ magnetic phase.

The sample was a high quality single crystal prepared, orientated and polished at Warwick. The orthorhombic *b*-axis was normal to the polished surface. The study concentrated on the Sm L_2 edge (~ 7.32 keV), where the strongest magnetic scattering would be expected in the system. Guided by information from scattering studies on TbMnO_3 [2], we have been successful in finding magnetic satellite reflections in $\text{Sm}_{0.5}\text{Y}_{0.5}\text{MnO}_3$. Indeed, we have observed (resonant) satellites corresponding to the four domain types, A-, F-, C- and G-type, reported from RXS studies on TbMnO_3 [2]. We show their temperature dependences in Figure 22. The wavevector corresponding to these four reflections is $q \approx 0.32 b^*$, which is close to the value ($q_{\text{Mn}} \approx 0.28\text{--}0.29 b^*$) associated with the ordering of the Mn 3d moments in TbMnO_3 [2].

By inference from the RXS, non-RXS and neutron diffraction results on TbMnO_3 [2], we believe that the

scattering we have observed here (Figure 22) is an indirect response from the ordering of the Mn 3d moments, seen via their polarization of the Sm 5d band. That is, we infer that $q_{\text{Mn}} \approx 0.32 b^*$ in $\text{Sm}_{0.5}\text{Y}_{0.5}\text{MnO}_3$. Like the Tb 4f moments in TbMnO_3 , it is possible that the Sm 4f moments order at a much lower temperature with their own (distinct from Mn order) wavevector. It will be our goal in future XMaS studies to hunt out such ordering. ■

[1] D. Khomskii, *Physics* 2, 20 (2009).

[2] D. Mannix et al., *Phys. Rev. B* 76, 184420 (2007) and O. Prokhnenko et al., *Phys. Rev. Lett.* 99, 177206 (2007). (Both of these articles include data from XMaS.)

[3] D. O'Flynn et al., *J. Phys: Proceedings of ICM* (2009).

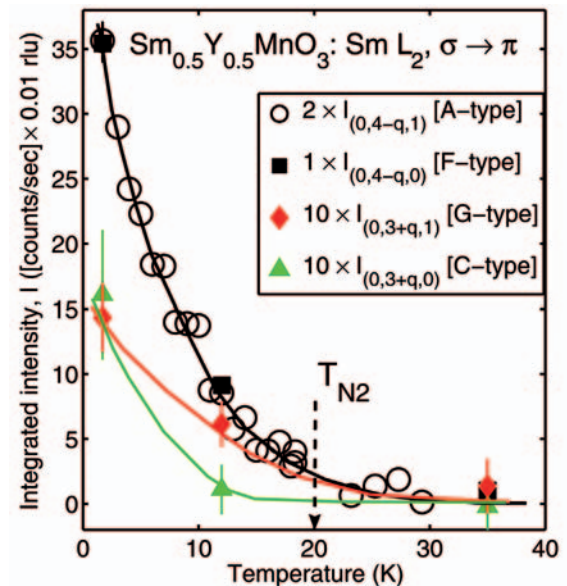


Figure 22: Temperature dependence of the integrated intensities of the different magnetic satellite reflections observed in $\text{Sm}_{0.5}\text{Y}_{0.5}\text{MnO}_3$, recorded at the Sm L_2 absorption edge in the rotated polarization channel ($\sigma \rightarrow \pi$). The labels A, C, F and G follow a convention used in studies of TbMnO_3 (see Ref. [2]). Solid lines are guides to the eye. The vertical dashed line indicates the temperature at which a second magnetic transition and an anomaly in the dielectric constant are found coincident with each other in bulk studies (Ref. [3]).

➔ Please note

Some of the experimental reports in the previous pages are as yet unpublished. Please email the contact person if you are interested in any of them or wish to quote these results elsewhere.

➔ Our web site

This is at:

<http://www.esrf.fr/UsersAndScience/Experiments/CRG/BM28/>

It contains the definitive information about the beamline and the on-line beamline manual.

➔ Living allowances

These are still 55 euros per day per beamline user—the equivalent actually reimbursed in pounds sterling, of course. XMaS will support up to 3 users per experiment. This is not a restriction on the number of experimentalists but you should make your own budgetary arrangements for those in excess of 3. The ESRF hostel still appears adequate to accommodate all our users, though CRG users will always have a lower priority than the ESRF's own users. Do remember to complete the web-based "A form" requested of you when you receive the ESRF invitation, all attendees must be listed, since this informs the safety group of the attendees and is used to organise all site passes, meal cards and accommodation.

➔ Beamline people

The personnel changes which occurred during 2009 were described by Malcolm and Chris in the Introduction to this Newsletter.

Beamline Responsible – ESRF require all CRGs to nominate the local team member responsible for the CRG. Simon Brown (sbrown@esrf.fr), as the senior scientist in the team, has taken over the role of Beamline Responsible from David Paul.

Beamline Coordinator – Laurence Bouchenoire, (boucheno@esrf.fr), is the person who can provide you with general information about the beamline, application procedures, scheduling, etc. Laurence should normally be your first point of contact.

Beamline Scientists – Simon Brown (sbrown@esrf.fr), Peter Normile (normile@esrf.fr) and Oier Bikondoa (oier.bikondoa@esrf.fr).

Technical Support – Paul Thompson (pthomps@esrf.fr) continues to work on instrument development and provides technical support for the beamline. John Kervin (jkervin@liv.ac.uk), who is based at Liverpool University, provides further technical back-up and spends part of his time on-site at XMaS.

Project Directors – Malcolm Cooper (m.j.cooper@warwick.ac.uk) and Chris Lucas (clucas@liv.ac.uk) continue to travel between the UK and France to oversee the operation of the beamline. The administration for XMaS continues to be handled by Sandra Beaufoy at Warwick University (s.beaufoy@warwick.ac.uk).

➔ The Project Management Committee

The current membership of the committee is as follows:

- Bob Cernik (chair)
- Denis Greig
- Peter Hatton
- Chris Nicklin
- David Bradley
- Andrew Boothroyd
- Colin Norris
- Jonathan Williams

meeting twice a year, in addition to the above, the directors, the chair of the PRP and the beamline team are in attendance.

➔ The Peer Review Panel

The current membership of the panel is as follows:

- Sean Langridge (chair)
- Paul Strange
- Carsten Detlefs
- Steve Collins
- Pam Thomas
- Ian Hamley
- Karen Edler

In addition either Malcolm Cooper or Chris Lucas attends their meetings.

➔ Housekeeping!!

At the end of your experiment samples should be removed, tools, etc returned to racks and unwanted materials disposed of in appropriately. When travel arrangements are made, therefore, please allow additional time to effect a tidy-up.

➔ PUBLISH PLEASE!!... ...and keep us informed

Although the list of XMaS papers is growing we still need more of those publications to appear. We ask you to provide Sandra Beaufoy not only with the reference but also a preprint/reprint for our growing collection. Note that the abstract of a publication can also serve as the experimental report!

➔ IMPORTANT!

When beamline staff have made a significant contribution to your scientific investigation you may naturally want to include them as authors.

Otherwise we ask that you add an acknowledgement, of the form:

"This work was performed on the EPSRC-funded XMaS beamline at the ESRF, directed by M.J. Cooper and C.A. Lucas. We are grateful to the beam line team of S.D. Brown, P. Normile, O. Bikondoa, L. Bouchenoire and P. Thompson for their invaluable assistance, and to S. Beaufoy and J. Kervin for additional support."



Guidelines for Beam-time applications

Beamline Operation

The XMaS beamline at the ESRF, which came into operation in April 1998, has some 133 days of beam time available each year for UK user experiments, after deducting time allocated for ESRF users, machine dedicated runs and maintenance days. During the year, two long shut-downs of the ESRF are planned: 4 weeks in winter and 4 weeks in summer. At the ESRF, beam is available for user experiments 24 hours a day.

Applications for Beam Time

Two proposal review rounds are held each year, with deadlines for submission of applications, normally, the end of March and September for the scheduling periods August to end of February, and March to July, respectively. Applications for Beam Time are to be submitted electronically (the paper versions are not acceptable) following the successful model used by the ESRF and ourselves. Please consult the instructions given in the ESRF web page:

www.esrf.fr

Follow the links: “**User Portal**”
under “**Quick Links**”

Enter your surname and password
and select: “**Proposals/Experiments**”

Follow the instructions carefully — you must choose “CRG Proposal” and “XMAS-BM28” at the appropriate stage in the process. A detailed description of the process is always included in the reminder that is emailed to our users shortly before the deadline – for any problems contact L. Bouchenoire, as above.

Technical specifications of the beamline and instrumentation available are described in the XMaS web page. When preparing your application, please consider the following:

➡ All sections of the form must be filled in. Particular attention should be given to the safety aspects, and the name and characteristics of the substance completed carefully. Experimental conditions requiring special safety precautions such as the use of lasers, high pressure cells, dangerous substances, toxic substances and radioactive

materials, must be clearly stated in the proposal. Moreover, any ancillary equipment supplied by the user must conform with the appropriate French regulations. Further information may be obtained from the ESRF Experimental Safety Officer, tel: +33 (0)4 76 88 23 69; fax: +33 (0)4 76 88 24 18.

➡ Please indicate your date preferences, including any dates that you would be unable to attend if invited for an experiment. This will help us to produce a schedule that is satisfactory for all.

➡ An experimental report on previous measurements must be submitted. New applications will not be considered unless a report on previous work is submitted. These also should be submitted electronically, following the ESRF model. The procedure for the submission follows that for the submission of proposals – again, follow the instructions in the ESRF’s web pages carefully. Reports must be submitted within 6 months of the experiment.

➡ The XMaS beamline is available for one third of its operational time to the ESRF’s user community. Applications for beamtime within that quota should be made in the ESRF’s proposal round - **Note: their deadlines are earlier than for XMaS! - 1st March and 1st September.** Applications for the same experiment may be made both to XMaS directly and to the ESRF. Obviously, proposals successfully awarded beamtime by the ESRF will not then be given beamtime additionally in the XMaS allocation.

Assessment of Applications

The Peer Review Panel for the UK-CRG considers the proposals, grades them according to scientific excellence, adjusts the requested beam time if required, and recommends proposals to be allocated beam time on the beamline.

Proposals which are allocated beam time must in addition meet ESRF safety and XMaS technical feasibility requirements.

Following each meeting of the Peer Review Panel, proposers will be informed of the decisions taken and some feedback provided.

XMaS, ESRF, 6, rue Jules Horowitz BP 220, 38043 Grenoble Cedex, France
Tel: +33 (0)4 76 88 24 36 – Fax: +33 (0)4 76 88 24 55
Web page : http://www.esrf.fr/exp_facilities/BM28/xmas.html
Email: boucheno@esrf.fr



is an EPSRC sponsored project

